High resolution U□Pb dating of Middle Triassic volcaniclastics: Time-scale calibration and verification of tuning parameters for carbonate sedimentation

Article *in* Earth and Planetary Science Letters · July 1996

DOI: 10.1016/0012-821X(96)00057-X

CITATIONS
185

READS
103

5 authors, including:

Peter Brack
ETH Zurich
73 PUBLICATIONS **2,920** CITATIONS

SEE PROFILE

ELSEVIER

Earth and Planetary Science Letters 141 (1996) 137–151

EPSL

High resolution U–Pb dating of Middle Triassic volcaniclastics: Time-scale calibration and verification of tuning parameters for carbonate sedimentation

Roland Mundil [a,*], Peter Brack [b,1], Martin Meier [a,2], Hans Rieber [c,3], Felix Oberli [a,4]

[a] *Institute of Isotope Geology and Mineral Resources, ETH-Zentrum, NO H 45, CH-8092 Zürich, Switzerland*
[b] *Department of Earth Sciences, ETH-Zentrum, NO E 17.1, CH-8092 Zürich, Switzerland*
[c] *Institute and Museum of Palaeontology, Zürich University, Karl Schmid-Strasse 4, CH-8006 Zürich, Switzerland*

Received 2 October 1995; accepted 15 March 1996

Abstract

We report high-resolution single-zircon U–Pb age data for Middle Triassic volcaniclastic intercalations in biostratigraphically calibrated pelagic successions of the Southern Alps. The results require a redefinition of the chronometric scale for the Middle Triassic. Moreover, they do not support current models relating cyclic sedimentation in platform carbonates of the Dolomites to orbital tuning.

Tight concordant age clusters were obtained for five volcaniclastic layers in three ammonoid biozones of late Anisian to early Ladinian age. Two layers in the (Nevadites) Secedensis Zone yielded identical mean $^{206}Pb/^{238}U$ ages of $241.2 + 0.8/-0.8$ Ma and $241.2 + 0.8/-0.6$ Ma (errors given at the 95% confidence level). A layer in the Gredleri Zone is dated at $238.8 + 0.5/-0.2$ Ma, and two horizons in the Archelaus Zone yield similar ages of $237.9 + 1.0/-0.7$ Ma and $238.0 + 0.4/-0.7$ Ma. These results are significantly older than the age values of 233–235 Ma assigned to the Anisian/Ladinian boundary by several current time scales [1–4]. Moreover, our estimate of 240.7–241.3 Ma (depending on biostratigraphic collocation) for the Anisian/Ladinian boundary casts doubts on the reliability of age values of 245–250 Ma proposed by most time scales for the Permian/Triassic boundary.

The occurrence of pelagic fossils in basinal sediments as well as in age-equivalent shallow marine Middle Triassic platform carbonates in the Dolomites allows the sedimentary sequences of both environments to be correlated. The 800 m thick Latemar platform (western Dolomites) is characterized by cyclic stacking patterns, which have been interpreted as results of Milankovitch-type high-frequency/low-amplitude sea-level fluctuations. The 12 m.y. interval of platform growth postulated from the assignment of orbital periodicities to the platform carbonate cycles [5,6] is in conflict with a maximum time span of 4.7 m.y. allowed by the present zircon data.

Keywords: Anisian; Ladinian; Latemar Massif; U/Pb; pyroclastics

* Corresponding author. Fax: +41 1 632 11 79, E-mail: mundil@igmr.erdw.ethz.ch
[1] Fax: +41 1 632 10 88, E-mail: brack@erdw.ethz.ch.
[2] Fax: +41 1 632 11 79, E-mail: meier@igmr.erdw.ethz.ch.
[3] Fax: +41 1 262 59 37.
[4] Fax: +41 1 632 11 79, E-mail: oberli@igmr.erdw.ethz.ch.

PII S0012-821X(96)00057-X

1. Introduction

Reliable radiometric age determinations are rare for the entire Triassic stage [1–4,7]. Even the most recent time scale [4] relies on virtually the same database for Triassic times as [7]. Both scales, however, propose different ages for stage boundaries. To date, Middle Triassic time scales have been mainly based on K–Ar and $^{40}Ar/^{39}Ar$ ages [8] and on K–Ar and Rb–Sr ages [9,10] from magmatic products in the Southern Alps. The uncertainties of these ages, however, vary between 2% and 4% (2σ error).

The most promising objects for precise time-scale calibration are volcano-derived airborne deposits interbedded within biostratigraphically calibrated sedimentary successions. In this study, high-resolution conventional single-zircon U–Pb age dating techniques have been applied to obtain precise and accurate ages for several volcaniclastic horizons in the Southern Alps. Zircon occurs as a trace constituent in many acidic volcaniclastics and is relatively stable in the sedimentary environment. This mineral is highly suitable for the purpose of dating sedimentary sequences, because its crystallisation age closely approximates the times of volcanic eruption and deposition. Complications arising from the presence of inherited older cores can be avoided or minimized by careful selection and microscopic inspection prior to analysis. Single-crystal analysis of samples containing cryptic, undetected older cores typically produces results which are resolved from those of samples devoid of inheritance and are thus readily rejected. If the effects of secondary loss of radiogenic Pb are minimized by air-abrasion techniques [11], single-grain data from a volcaniclastic layer typically result in a tight cluster of Pb/U ages and thus define highly precise ages for deposition. Control of laboratory contamination at low Pb levels and the use of a linear secondary electron multiplier for the measurement of small ion beams result in a precision of the $^{206}Pb/^{238}U$ age better than 1 Ma (95% confidence level) for individual age determinations on Middle Triassic single zircon crystals with radiogenic Pb contents of 3.2–240 pg (10^{-12} g).

Middle Triassic pelagic sediments containing zircon-bearing acidic volcaniclastic horizons are widespread in the Southern Alps. Samples were taken from volcaniclastic layers in sections with tight biostratigraphic control, which can be correlated in detail over long distances (> 200 km) [12]. Moreover, the pelagic successions can be correlated biostratigraphically and geometrically with carbonate platforms in the Dolomites (Fig. 5). Some of the platform successions are characterized by conspicuous regular stratal patterns in their interior parts. In particular, the Latemar platform in the western Dolomites has been presented as a prominent example of Milankovitch-type cyclicities recorded in platform carbonates of the older Mesozoic [5,6].

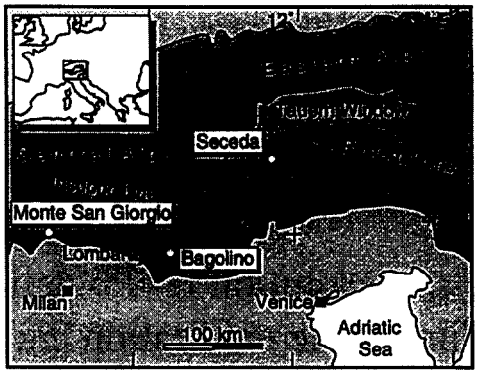

Fig. 1. Overview of the Southern Alps and neighbouring areas with sampling locations.

The main goals of this study were two-fold: (1) to recalibrate and redefine the Middle Triassic chronometric scale; and (2) to evaluate critically the orbital tuning hypothesis used to explain sedimentary patterns observed in the Latemar carbonate platform.

2. Geological framework

The non-metamorphic Southern Alps (Fig. 1) consist of slices of basement units and mainly Mesozoic cover rocks thrust to the south. To the north they are bound by the Insubric–Pustertal Line. During the latest Anisian to early Ladinian, several carbonate platforms were simultaneously aggrading in the Dolomites. Age-equivalent starved pelagic successions (Buchenstein Beds) accumulated in narrow basinal areas between these platforms. To the west of this region, in eastern Lombardy, pelagic successions were deposited in a more open marine environment.

2.1. Volcaniclastics

Volcaniclastic intercalations ('Pietra Verde') predominantly occur in the Buchenstein Beds. These volcaniclastics are considered to be products of an explosive, acidic (rhyolitic to rhyodacitic) volcanism [13]. Their wide spatial distribution suggests that a number of volcanic centres existed throughout the western Tethys, even though only a few potential sites have been discovered to date.

In Lombardy and in the northwestern Dolomites, the Pietra Verde volcaniclastics are only a centimetres to decimetres thick and contain as phenocrysts mainly quartz, feldspar, biotite and subordinate quan-

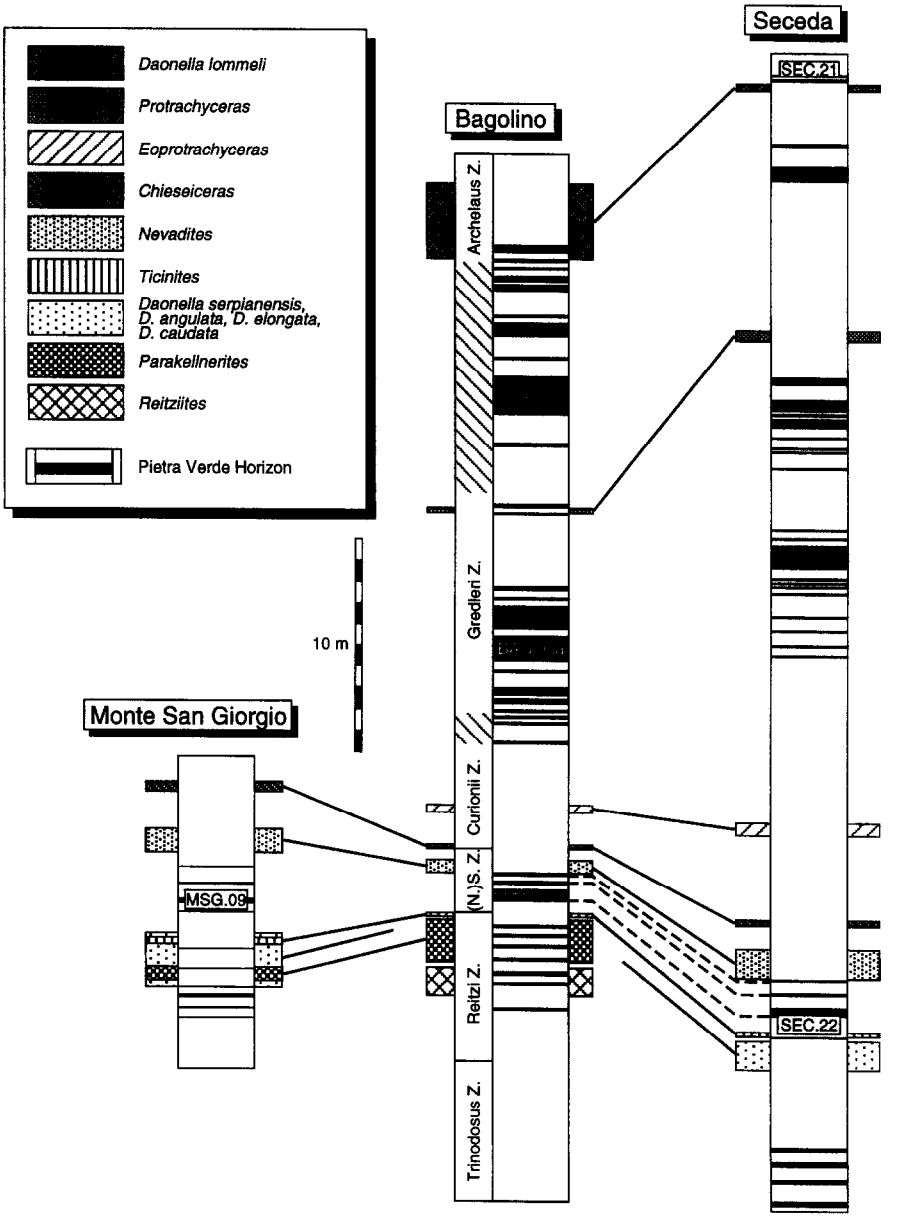

Fig. 2. Correlated sections of sampling locations with the distribution of ammonoid genera and bivalves of genus *Daonella* (solid lines) as well as volcaniclastic layers (dashed lines). For details see [12,19].

tities of ore minerals, apatite and zircon. In the vicinity of minor eruption centres in Eastern Lombardy, the volcaniclastic layers reach a thickness of several metres and comprise large lava clasts. Most of the finer-grained volcaniclastics were presumably transported in an eruption cloud before being deposited as fallout particles. The occurrence of accretionary lapilli in several tuff layers (e.g. [14] and

Table 1
Single-zircon U–Pb isotopic data from five samples

sample/ grain no.	weight (μg)	original cystal size (L · W in μm)	degree of abrasion[a]	U conc. (ppm)	Pb rad. (pg)	Pb common[b] (pg)	$^{206}Pb/^{204}Pb$[c]	$^{208}Pb/^{206}Pb$[d]
SEC.22								
Z101	6.4	415 · 210	34	174	44.5	5.8	467	.1731 ± 9
Z102	21.0	320 · 230	16	179	146.7	5.8	1542	.1426 ± 4
Z103	3.7	415 · 210	45	120	18.1	3.8	286	.2094 ± 30
Z104	20.0	435 · 185	3	264	210.9	5.7	2144	.1917 ± 4
Z105	15.5	595 · 265	36	157	92.4	4.4	1281	.1135 ± 5
Z106	15.3	295 · 205	14	225	134.8	4.3	1866	.1527 ± 4
Z107	9.6	325 · 195	26	219	84.7	3.2	1522	.1746 ± 6
Z108	20.6	475 · 215	15	161	135.7	6.3	1260	.1942 ± 5
Z110	30.4	415 · 135	0	134	162.0	4.5	2034	.2042 ± 4
Z201	3.0	300 · 140	26	158	20.2	2.8	402	.2486 ± 19
Z202	5.0	325 · 165	30	104	20.9	3.1	399	.1656 ± 18
MSG.09								
Z102	0.8	245 · 85	25	348	11.2	4.2	174	.1791 ± 35
Z104	0.8	187 · 95	31	390	13.0	5.4	152	.2398 ± 36
Z105	2.9	150 · 160	0	401	44.1	4.4	588	.2091 ± 11
Z107	0.5	145 · 105	46	163	3.2	4.6	59	.1337 ± 148
Z108	0.8	180 · 85	64	411	13.8	4.2	201	.2230 ± 34
Z110	1.0	310 · 90	24	291	12.2	4.6	166	.2175 ± 36
BAG.06a								
Z102	22.2	375 · 185	0	173	151.2	11.2	815	.1648 ± 7
Z104	12.8	305 · 235	35	239	119.9	12.5	592	.1540 ± 8
Z105	34.6	405 · 160	0	182	241.1	12.5	1153	.1755 ± 5
Z109	15.2	355 · 185	5	196	118.1	21.7	342	.1737 ± 9
Z110	3.4	315 · 145	31	263	35.8	6.5	335	.1843 ± 21
Z112	1.6	230 · 195	55	340	21.9	4.9	271	.1845 ± 33
Z203	9.4	375 · 105	0	197	71.4	7.1	583	.2186 ± 11
Z204	8.2	395 · 100	5	271	87.4	7.0	740	.2025 ± 12
BAG.07								
Z101	3.0	380 · 110	12	179	21.6	5.7	234	.1898 ± 32
Z106	5.4	480 · 100	5	209	44.7	3.8	675	.2058 ± 14
Z111	4.8	340 · 115	3	334	60.2	6.6	568	.1304 ± 12
Z115	9.0	395 · 145	4	338	117.0	5.4	1302	.1495 ± 7
Z201	3.6	365 · 116	14	222	31.1	4.7	403	.1529 ± 21
Z204	2.1	330 · 115	28	136	11.6	3.8	188	.1989 ± 47
Z207	1.2	355 · 110	35	265	13.0	3.1	249	.2162 ± 35
SEC.21								
Z101	6.5	340 · 175	25	136	36.8	4.2	506	.2076 ± 16
Z102	9.3	425 · 165	15	241	90.8	3.8	1358	.2060 ± 8
Z106	7.5	405 · 150	8	139	42.2	5.7	431	.2215 ± 18
Z111	9.5	355 · 185	18	187	73.8	5.1	821	.2284 ± 11
Z115	5.0	380 · 170	34	211	42.9	4.7	531	.2081 ± 17
Z202	3.0	275 · 110	11	179	21.9	3.7	348	.2070 ± 32
Z204	5.6	250 · 185	33	242	54.5	10.8	307	.2036 ± 17
Z209	3.7	355 · 145	28	78	11.5	5.0	149	.1794 ± 69
Z216	10.3	390 · 255	44	209	87.1	6.8	745	.2037 ± 15
Z219	12.2	350 · 190	17	179	88.4	4.6	1095	.2061 ± 9
Z301a	25.4	405 · 170	0	181	182.3	5.6	1869	.1926 ± 6
Z301b	3.3	180 · 210	40	155	20.4	3.9	315	.1641 ± 28

[a] Size reduction by air abrasion in percentage of the original width of the crystals. [b] Total common Pb in analysis including analytical blank and tracer contribution. [c] Measured value corrected for secondary electron multiplier (SEM) mass discrimination and fractionation. [d] Ratios of radiogenic Pb and Pb versus U; data corrected for SEM mass discrimination and fractionation, tracer contribution, laboratory Pb blank and 240 Ma sample common Pb contribution, adopting model III of [26].

own observations) confirms their airborne origin. The fact that a number of distinct thin ash layers can be traced over long distances and across different basins further supports the interpretation of these layers as primary volcaniclastic horizons [12].

2.2. Basin–platform relationships and platform cycles

During the late Anisian/early Ladinian, carbonate platforms in the Dolomites reached a thickness of

Table 1 (continued)

$^{207}Pb/^{206}Pb$ [d]	$^{207}Pb/^{235}U$ [d]	$^{206}Pb/^{238}U$ [d,e]	ρ [f]	$^{207}Pb/^{235}U$ age (Ma)	$^{206}Pb/^{238}U$ age (Ma) [e]
.05121 ± 35	.2684 ± 20	.03804 ± 7	.52	241.4 ± 1.6	240.64 ± 0.44
.05115 ± 13	.2688 ± 10	.03812 ± 8	.72	241.7 ± 0.8	241.19 ± 0.51
.05202 ± 127	.2706 ± 70	.03773 ± 11	.56	243.1 ± 5.6	238.77 ± 0.71
.05111 ± 12	.2627 ± 9	.03733 ± 8	.75	237.0 ± 0.7	236.28 ± 0.48
.05100 ± 18	.2674 ± 11	.03805 ± 4	.62	240.6 ± 0.9	240.72 ± 0.26
.05104 ± 15	.2663 ± 11	.03786 ± 8	.67	239.8 ± 0.9	239.54 ± 0.52
.05137 ± 20	.2708 ± 13	.03824 ± 8	.60	243.3 ± 1.0	241.92 ± 0.51
.05128 ± 14	.2694 ± 10	.03811 ± 7	.70	242.2 ± 0.8	241.12 ± 0.42
.05115 ± 11	.2594 ± 8	.03680 ± 6	.77	234.2 ± 0.6	232.94 ± 0.40
.05142 ± 75	.2704 ± 42	.03815 ± 9	.48	243.0 ± 3.4	241.34 ± 0.58
.05111 ± 70	.2695 ± 40	.03825 ± 9	.48	242.3 ± 3.2	242.00 ± 0.55
.05188 ± 146	.2720 ± 81	.03804 ± 13	.50	244.3 ± 6.4	240.68 ± 0.78
.05166 ± 148	.2673 ± 81	.03754 ± 16	.49	240.5 ± 6.5	237.57 ± 1.01
.05164 ± 40	.2486 ± 23	.03493 ± 13	.54	225.4 ± 1.8	221.34 ± 0.82
.04982 ± 602	.2608 ± 332	.03799 ± 35	.71	235.3 ± 26.7	240.36 ± 2.18
.05153 ± 150	.2714 ± 82	.03821 ± 13	.41	243.8 ± 6.6	241.74 ± 0.81
.05284 ± 147	.2786 ± 82	.03825 ± 12	.55	249.6 ± 6.5	241.99 ± 0.77
.05109 ± 25	.2650 ± 15	.03763 ± 6	.55	238.7 ± 1.2	238.13 ± 0.37
.05129 ± 27	.2669 ± 16	.03776 ± 6	.56	240.2 ± 1.3	238.94 ± 0.40
.05122 ± 17	.2556 ± 10	.03621 ± 6	.64	231.1 ± 0.8	229.27 ± 0.35
.05108 ± 29	.2657 ± 18	.03773 ± 9	.59	239.2 ± 1.4	238.76 ± 0.56
.05100 ± 82	.2652 ± 45	.03772 ± 8	.52	238.8 ± 3.6	238.70 ± 0.47
.05141 ± 132	.2680 ± 72	.03782 ± 11	.55	241.1 ± 5.8	239.33 ± 0.65
.05111 ± 40	.2483 ± 21	.03525 ± 5	.54	225.2 ± 1.7	223.32 ± 0.30
.05111 ± 46	.2623 ± 26	.03724 ± 9	.45	236.5 ± 2.1	235.68 ± 0.58
.05155 ± 126	.2675 ± 69	.03766 ± 11	.52	240.7 ± 5.5	238.28 ± 0.70
.05154 ± 58	.2603 ± 31	.03665 ± 9	.43	234.9 ± 2.5	232.02 ± 0.55
.05147 ± 46	.2619 ± 26	.03692 ± 9	.46	236.2 ± 2.0	233.70 ± 0.56
.05122 ± 24	.2631 ± 15	.03728 ± 8	.55	237.2 ± 1.2	235.94 ± 0.47
.05165 ± 81	.2668 ± 44	.03748 ± 9	.48	240.2 ± 3.6	237.20 ± 0.58
.05129 ± 188	.2669 ± 103	.03776 ± 16	.52	240.2 ± 8.3	238.92 ± 0.96
.05140 ± 145	.2660 ± 79	.03754 ± 12	.51	239.5 ± 6.3	237.59 ± 0.74
.05152 ± 64	.2742 ± 36	.03861 ± 10	.45	246.0 ± 2.9	244.23 ± 0.59
.05116 ± 28	.2643 ± 16	.03748 ± 8	.51	238.1 ± 1.3	237.20 ± 0.51
.05151 ± 67	.2630 ± 37	.03705 ± 9	.47	237.1 ± 3.0	234.50 ± 0.55
.05116 ± 39	.2657 ± 22	.03768 ± 8	.48	239.3 ± 1.8	238.44 ± 0.53
.05118 ± 71	.2656 ± 39	.03766 ± 10	.44	239.2 ± 3.2	238.29 ± 0.63
.05202 ± 139	.2705 ± 76	.03773 ± 11	.52	243.1 ± 6.1	238.73 ± 0.70
.05156 ± 65	.2648 ± 36	.03727 ± 8	.50	238.6 ± 2.9	235.89 ± 0.53
.05245 ± 291	.2711 ± 158	.03750 ± 18	.62	243.5 ± 12.6	237.29 ± 1.09
.05146 ± 57	.2665 ± 32	.03758 ± 11	.48	239.9 ± 2.6	237.80 ± 0.68
.05120 ± 31	.2646 ± 18	.03750 ± 6	.49	238.4 ± 1.4	237.29 ± 0.40
.05125 ± 17	.2620 ± 11	.03709 ± 7	.63	236.3 ± 0.9	234.77 ± 0.46
.05137 ± 115	.2664 ± 63	.03763 ± 13	.46	239.8 ± 5.1	238.11 ± 0.83

[e] $^{206}Pb/^{238}U$ ratios and $^{206}Pb/^{238}U$ age values corrected by $+1 \cdot 10^{-5}$ to $+2 \cdot 10^{-5}$ or +80 to +90 ka, respectively, for initial disequilibrium in $^{230}Th/^{238}U$, adopting Th/U = 3.6 for the crystallisation environment. [f] Correlation coefficient of radiogenic $^{207}Pb/^{235}U$ versus $^{206}Pb/^{238}U$. Uncertainties are given at the 95% confidence level. Uncertainties for the isotopic ratios refer to the least significant digits of the corresponding values.

~ 800 m (e.g. [15]). Fossiliferous beds in the interior parts and on the slopes of the Latemar carbonate platform contain pelagic fossils [12] suitable for correlation with age-equivalent basinal successions (Buchenstein Beds, Fig. 5). Volcaniclastic layers (Pietra Verde) occur throughout the entire succession of the Buchenstein Beds. The growth period of the coeval platform carbonates can therefore be inferred from absolute age determinations on zircons from Pietra Verde layers.

Parts of the platform interior are characterized by regular cyclic stacking patterns. These have been interpreted as results of high-frequency/low-amplitude sea level fluctuations [5]. Graphic space–time analyses (Fischer plots, [16]) and spectral analyses [6] suggest superposition of several distinct frequen-

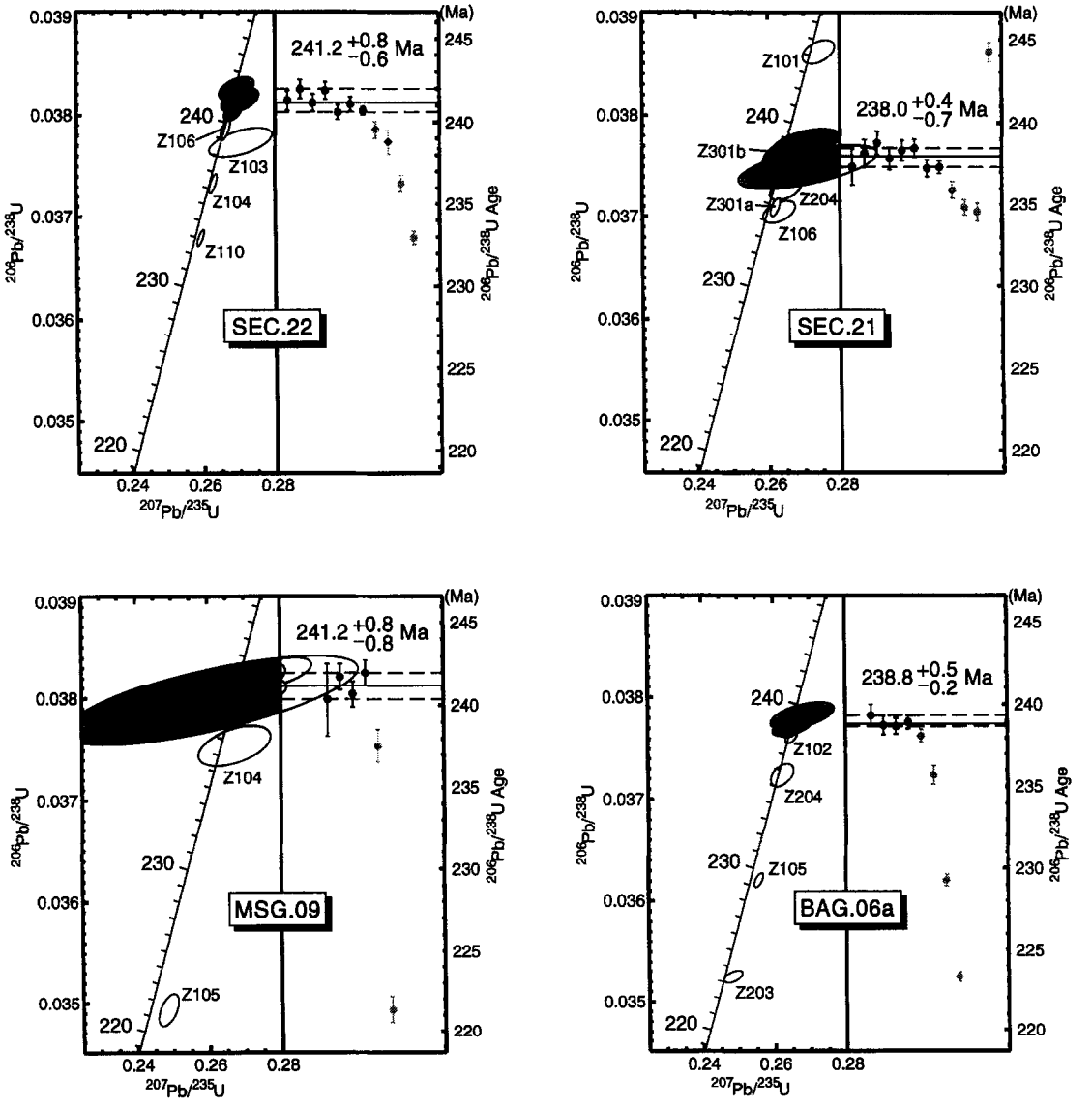

Fig. 3. Concordia representations of U–Pb data. The mean ages are calculated from the $^{206}Pb/^{238}U$ ages of zircons form the shaded cluster (error bars displayed in the right-hand part of the diagrams).

cies comparable to those reported from the Pleistocene [17]. Subrecent sea-level fluctuations are controlled by alternating cycles of glaciation and deglaciation as a function of variations in insolation, which, in turn, is controlled by the orbital parameters of the earth [18]. For the Latemar platform, Goldhammer and co-workers [5,6] explained the characteristic cyclic stacking patterns by the superposition of the 20 ka precession period and the 100 ka eccentricity period. The 600 cycles (= highest order units) reported in [5] multiplied by the 20 ka precession period yields a duration of 12 m.y. for the time interval of platform growth.

3. Sampling locations, biostratigraphic record and U–Pb age results

Samples were taken from three well-correlated South Alpine sections (Seceda, Bagolino and Monte San Giorgio). In these sections ammonoids, thin-shelled bivalves (genus *Daonella*) and conodonts document a time interval between the late Anisian Trinodosus Zone and late Ladinian Archelaus Zone (Fig. 2) ([12,19–21]; for correlation with low-latitude successions in North America, see also [22]).

At **Seceda** (northwestern Dolomites) the basal Buchenstein Beds consist of well-stratified bituminous limestones (Lower Plattenkalke). These are overlain by pelagic siliceous nodular limestones (Knollenkalke) and more evenly bedded, partly dolomitized, turbiditic limestones (Upper Bänderkalke) in the upper part. Several thin Pietra Verde horizons can be correlated individually with those of the Bagolino section (Fig. 2).

At **Bagolino** (eastern Lombardy) pelagic limestones (Knollenkalke) similar to those of Seceda are interstratified with Pietra Verde layers a few centimetres to decimetres thick. They are usually massive, phenocryst-rich and of greenish (fresh) to yellowish (weathered) colour. Due to advanced diagenetic overprint (> 150°C, presumably during the early Tertiary), zircons were strongly affected by secondary Pb loss.

At **Monte San Giorgio** (Ticino, Southern Switzerland) layers of bentonite a few millimetres to centimetres thick occur within an approximately 20 m thick intraplatform succession of fossil-rich dolostones and bituminous shales (Grenzbitumenzone, [23]). The bentonites consist of a microcrystalline matrix of illite–montmorillonite and contain phenocrysts of alkali feldspar, quartz and accessory zircon [8,24].

Table 2
Mean results and associated parameters based on different statistical models (see text)

Sample No.	1	2	3	4	5	6
SEC.21 (8 grains)	237.8	+0.4 −0.4	+0.5 −0.5	1.01	238.0	+0.4 −0.7
BAG.07 (4 grains)	237.8	+0.7 −0.7	+1.1 −1.1	1.00	237.9	+1.0 −0.7
BAG.06a (4 grains)	238.9	+0.5 −0.5	+0.4 −0.4	0.48	238.8	+0.5 −0.2
MSG.09 (4 grains)	241.4	+0.9 −0.9	+1.1 −1.1	0.78	241.2	+0.8 −0.8
SEC.22 (7 grains)	241.1	+0.3 −0.3	+0.5 −0.5	1.21	241.2	+0.8 −0.6

Results of U–Pb age dating are reported in stratigraphic order of the samples (Fig. 2). The isotopic data and age results are documented in Tables 1 and 2 and Fig. 3. Analytical procedures and data processing are described in Appendix A and Appendix B. The analytical uncertainties as listed in the tables and shown as error ellipses and error bars in the Figures are given at the 95% confidence level.

Sample SEC.22 is from the base of the 'Knollenkalke' exposed in the cliff section to the south of Seceda cable car station. The horizon belongs to the **(Nevadites) Secedensis Zone**. Based on detailed correlation, this layer is approximately age-equivalent with bed 71 (= MSG.09) at Monte San Giorgio. The layer contains medium to coarse sand size phenocrysts. Comparatively large crystals were selected for dating, most of which were euhedral, short-prismatic and clear. Needle/rod-shaped mineral inclusions and bubble/dumbbell-shaped, opaque inclusions of possibly devitrified magma were abundant. Due to the relatively large size of the grains, the radiogenic Pb content was sufficiently high to obtain precise U–Pb results. Seven analyses of well-abraded grains form a tight concordant cluster yielding a mean $^{206}Pb/^{238}U$ age of **241.2 + 0.8 / −**

0.6 Ma (Fig. 3). Two analyses (Z110 and Z104) were performed on non-abraded or only slightly abraded grains. The error ellipses of both samples are discordant and reflect the effects of secondary Pb loss. Similarly, the U–Pb data for the only moderately abraded grains Z103 and Z106 are also resolved from the cluster and thus not included in the calculation of the age.

Sample MSG.09 was taken in a small mine (Miniera Val Porina) at 820 m altitude south of the main peak of Monte San Giorgio and corresponds to bed 71 in [25]. Biostratigraphically, the horizon belongs to the lower part of the **(Nevadites) Secedensis Zone**. The sample contains small amounts of very small zircon grains. The euhedral crystals are mostly long prismatic and colourless. Only few mineral inclusions were observed (apatite in grain Z104); most grains comprise fine (several microns in size), opaque inclusions similar to those mentioned in the Seceda sample. Due to the low sample weight and corresponding low contents of radiogenic Pb (3.2 pg, Z107), the analytical errors are comparatively large. Four out of six analyses form a tight concordant cluster with a mean $^{206}Pb/^{238}U$ age of **241.2 + 0.8 / − 0.8 Ma** (Fig. 3). The U–Pb data of non-abraded grain Z105 are clearly discordant, as the error ellipse does not overlap with the concordia curve, in spite of the crystal being free of inclusions, clear and not disturbed by recognizable cracks. Similarly, grain Z104 was excluded from the calculation of the mean age, although the grain is abraded and the result is concordant within the error. The error ellipse of Z104 is clearly separated from the cluster formed by the remaining zircon results.

Sample BAG.06a is from the middle Buchenstein Beds in the Caffaro river bed near Bagolino (site B in [20]). The ~ 15 cm thick, massive horizon contains mainly medium sand size components (feldspar, quartz, biotite and secondary calcite). Biostratigraphically, this layer is located between beds with *Eoprotrachyceras margaritosum* below and layers with representatives of *Arpadites* and *Protrachyceras* above, and therefore probably belongs to the **Gredleri Zone**. Zircon crystals were mainly short-prismatic, grains Z203 and Z204 were long-prismatic. Only a few opaque inclusions were observed. Four abraded grains form a tight concordant cluster, yielding a mean $^{206}Pb/^{238}U$ age of **238.8 + 0.5 / − 0.2 Ma** (Fig. 3). The remaining zircons were not or only slightly abraded and show evidence of secondary Pb loss. The error ellipses of non-abraded euhedral grains Z105 and Z203 are clearly discordant, in spite of being clear and devoid of recognizable cracks. Grain Z102 was excluded for the calculation of the mean age as it was not sufficiently abraded (see Table 1).

Sample BAG.07 is from a stratigraphically higher level at the same location as BAG.06a. It contains fine sand size components but less biotite than BAG.06a. Biostratigraphically it is controlled by the occurrence of *Daonella pichleri* and *D. indica* [12], which may be assigned to the Archelaus Zone. The morphologies of the zircon grains of this sample differ slightly from those of the remaining zircon populations, as the {100} and {110} prisms occur in equal proportions (Appendix A). The content of inclusions is significantly higher in comparison with the other samples. This phenomenon is not reflected in a higher common Pb content. Needle- to rod-shaped mineral inclusions were observed, and the characteristic dumbbell-shaped opaque inclusions occur. A mean $^{206}Pb/^{238}U$ age of 237.9 + 1.0/ − 0.7 Ma is calculated from a cluster of four abraded grains. As shown by the spread of $^{206}Pb/^{238}U$ ages, removal of crystal parts affected by secondary Pb loss may not have been fully successful. This may be due to the abundance of inclusions and to the considerable diagenetic overprint suffered by the area.

Sample SEC.21 is from a 3 cm thick, massive layer of light-brownish colour in the uppermost Buchenstein Beds between Seceda peak and Pana Scharte. This horizon can be assigned to the **Archelaus Zone** as indicated by the occurrence of *Daonella lommeli*. The sample contains medium sand size components and comparatively large amounts of biotite and is of excellent quality, as its zircons are euhedral, clear and relatively large. A mean $^{206}Pb/^{238}U$ value of **238.0 + 0.4 / − 0.7 Ma** is obtained from a tight concordant cluster of eight analyses (Fig. 3). Zircon Z101 is to date the only example in this study with a cryptic inherited core not being recognized by transmitted light microscopy. The error ellipse of this zircon is clearly separated from the cluster, yielding an older apparent $^{206}Pb/^{238}U$ age of 244.2 Ma. As pyramids of zircons are typically free of inherited cores, a pyramid of grain Z301 was

prepared for analysis. For this task, the zircon was fragmented using the method described by [27]. Of these fragments a pyramidal termination was abraded. Its $^{206}Pb/^{238}U$ age of 238.1 ± 0.4 Ma (Z301b) conforms to the mean age defined by the data cluster. Samples Z106, Z204 and Z301a (a discordant non-abraded fragment of grain Z301) are resolved from the cluster and were therefore not included in the mean.

4. Discussion and conclusions

4.1. Discussion of zircon age results

Tight concordant clusters of single-zircon U–Pb results obtained on five volcaniclastic layers define precise age markers for three ammonoid biozones of Anisian to Ladinian age: 241.2 + 0.8/ − 0.8 Ma and 241.2 + 0.8/ − 0.6 Ma for the (Nevadites) Secedensis Zone, 238.8 + 0.5/ − 0.2 Ma for the Gredleri Zone, 237.9 + 1.0/ − 0.7 Ma and 238.0 + 0.4/ − 0.7 Ma for the Archelaus Zone. These ages constrain a time interval of 3.2 + 1.5/ − 1.2 m.y. between the biostratigraphically oldest and the youngest layer. It is important to note that the numeric ages of the samples are consistent with both their stratigraphic succession and lateral relationships.

The age results imply sedimentation rates of 3–10 m/Ma for the pelagic carbonate fraction of the Buchenstein Beds (not decompacted) (Fig. 4), which are typical values for pelagic sediments [28]. A duration of 1–3 m.y. can be derived from our data for the Grenzbitumenzone (Monte San Giorgio), which is in good agreement with estimates of 1–10 m.y. based on the accumulation of organic matter and assumptions made for primary organic productivity [23].

Age bias, due to reworking of older volcaniclastic deposits, yielding older apparent age values is unlikely in view of the composition and distribution of the volcaniclastics, as well as of the excellent consistency in our data set. The latter aspect is particularly well illustrated by the age results of 241.2 + 0.8/ − 0.6 Ma and 241.2 + 0.8/ − 0.8 Ma for samples SEC.22 and MSG.09, respectively, which occupy nearly identical stratigraphic positions in widely different paleo-environmental settings (see fig. 11 in [12]). The Grenzbitumenzone (Monte San Giorgio) and the Buchenstein Beds in the northwestern Dolomites belong to different basinal areas that were more than 200 km apart (Fig. 2). Our results therefore support the assumption that the mean ages defined by the clusters can be interpreted as crystallization age of the zircons analyzed and thus closely approximate the deposition age of their volcaniclastic host rocks.

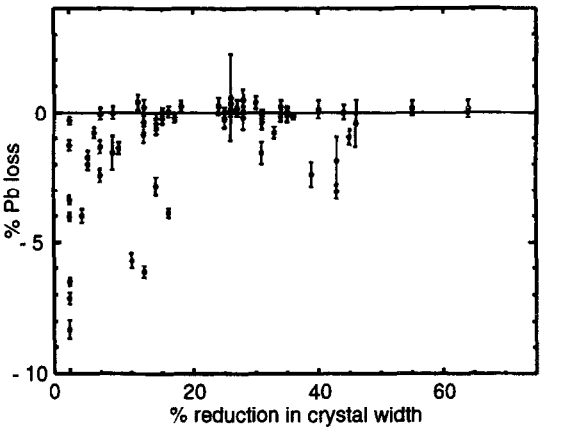

Fig. 4. Second-order least-squares fit of age data. The Bagolino section was taken as reference. The thickness of all volcaniclastic layers is reduced to zero. Arrows mark potential biostratigraphic collocations of the Anisian/Ladinian boundary and corresponding numeric ages.

A shift of the entire data set to older ages, due to hypothetical miscalibration of the mixed-tracer solution is excluded on the grounds of repeated independent tracer calibration, as well as by results obtained from a comparative study on natural zircon standards independently performed by three laboratories [29]. The trend to slightly younger apparent ages even within the clusters can be explained by a minor degree of Pb loss. Scatter, resulting from a possibly extended period of zircon crystallization in the magma chamber, may be superimposed on the data. As Pb loss is clearly the predominant source of scatter, we interpret our results as minimum ages.

4.2. Recalibration of time scale

The U–Pb single-zircon ages obtained in this study do not support previous age determinations on Middle Triassic Southern Alpine volcaniclastics

[8,30] and call for a revision of numeric values assigned to Middle Triassic stage boundaries.

Our precise mean age of 241.2 + 0.8/ − 0.8 Ma for sample MSG.09 only marginally agrees with the age value of 233 ± 9 Ma obtained by Hellmann and Lippolt [8] for high-sanidine from the same layer by K–Ar and $^{40}Ar/^{39}Ar$ techniques. This latter age has been used in most recent time scales as a key value for the chronometric definition of the Triassic time scale.

By interpolation/extrapolation of our data we propose ages of 240.7 Ma for the base of the Curionii Zone and 241.3 Ma for the base of the (Nevadites) Secedensis Zone (Fig. 4). Both markers are candidates for the collocation of the Anisian/Ladinian boundary. The boundary position still has to be agreed upon by the IUGS Subcommission on Triassic Stratigraphy [31].

Independently of the ultimate position of this boundary, the time interval remaining for the entire Early Triassic and Anisian is considerably smaller than 10 m.y., if values between 245 and 250 Ma are adopted for the Permian/Triassic boundary. In view of the detailed biostratigraphic subdivision of the Early to Middle Triassic of the Boreal realm (e.g. Siberia, see [32]) and the great thickness of coeval clastic successions in the Barents Sea [33], this time span appears to be extremely short.

Hence, our results do not only call for a redefinition of the Middle Triassic chronometric scale, but also suggest that age values between 245 and 250 Ma assigned to the Permian/Triassic boundary by the majority of recent time scales [1–4,7] might underestimate the true age of the boundary (see also [34]).

4.3. Assessment of tuning parameters for platform carbonate sedimentation

A striking result of this study is the significant discrepancy between our data and estimates of the duration of orbitally tuned platform carbonate sedimentation at Latemar. Based on their cycle counts and the apparent hierarchy in the stacking pattern (5:1 ratio) interpreted in terms of superposition of eccentricity and precession frequencies, Goldhammer and co-workers [5,6] propose a time interval of at least 12 m.y. for the growth of the cyclic platform portion (Fig. 5).

Sample SEC.22 (241.2 + 0.8/ − 0.6 Ma) lies stratigraphically close to the base of the cyclic succession and SEC.21 (238.0 + 0.4/ − 0.7 Ma) corresponds to a layer post-dating the cyclic sequence (see [35] for discussion and illustration of platform to basin relation). The duration of the cyclic portion of the Latemar platform is therefore constrained to 3.2 + 1.5/ − 1.0 m.y.. This is more than 60% shorter than the timespan obtained by applying frequencies of the Milankovitch spectrum. Significantly shorter orbital periods in Early Mesozoic times are unlikely. Extrapolations by Berger et al. [36] yield an only ~ 10% shorter precession period for the Triassic. Eccentricity appears to have been uniform during the earth's history.

Assuming that the succession is truly periodic and the cycle counts by Goldhammer et al. [5] are indeed

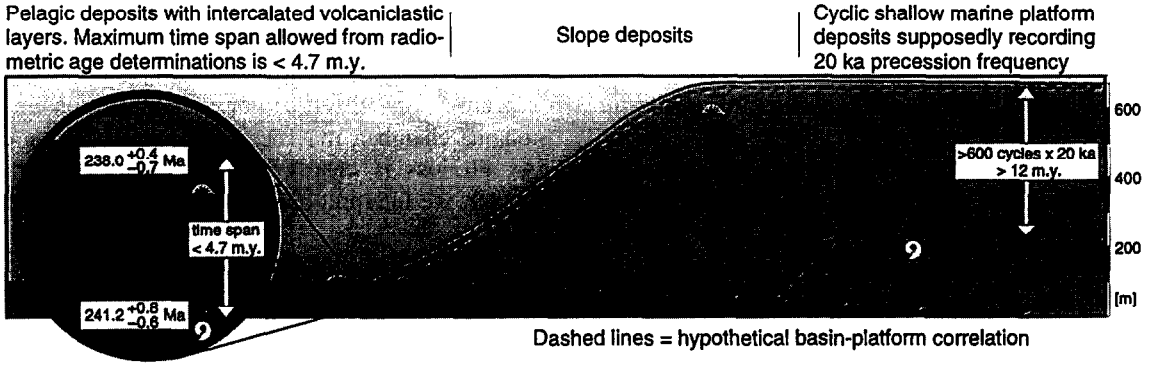

Fig. 5. Schematic section showing platform–basin correlation and constraining levels with radiometric data and age diagnostic fossils.

correct, the duration for each highest-order unit would be limited to < 8 ka by our data. No tuning mechanism with such a short period is known to date. In view of the restricted data set used for the spectral analysis by Hinnov and Goldhammer [6], the resulting specific periodicities may be accidental. We do not exclude the possibility that the succession of platform interior beds at Latemar might be partly non-periodic.

Shallow marine carbonate production and accumulation are sensitive to numerous global and local parameters. Because water depth is a major factor influencing carbonate production and redistribution, even minor (meter scale) shifts in sea-level strongly influence the mode of carbonate deposition, particularly on top of small platforms such as Latemar. Sea-level fluctuation of the order of a few meters was suggested by [5] for the generation of the highest-order units at Latemar. This is small compared to the large amplitudes of Pleistocene glacio-eustatic sea-level changes. Low-amplitude relative sea-level changes resulting from additional (non-orbitally driven) causes thus might have been of greater importance in periods devoid of extensive polar glaciations such as the Middle Triassic and could, therefore, have obliterated a potential record of orbital signals. In Pleistocene times similar minor signals, if existing, would have been largely suppressed by the high amplitudes of the oscillations caused by the build-up and decay of large ice caps, which were governed by orbital parameters.

Apparent hierarchies in cyclic stacking patterns; that is, generation of higher-order units from a single-periodicity sea-level signal, could also result from the complex interaction of threshold parameters of carbonate production and rates of sedimentation in response to relative sea-level changes [37]. Moreover, the growth of Middle Triassic platforms in the Southern Alps could have been affected by a combination of several local parameters influencing the stacking patterns of platform-interior beds:

(1) Small-scale subsidence/uplift due to tectonic activity and resulting in meter scale relative sea-level variations may have occurred, because the area of the Dolomites had been subjected to several phases of tectonism shortly before and deformation combined with magmatic activity immediately after platform growth (i.e. during the middle/late Anisian and late Ladinian, respectively). On the basis of a comparative study of age-equivalent sections in different platforms in the Dolomites we suspect that the apparent long-term (third-order) fluctuation with amplitudes of ~ 60 m (after correction for isostatic loading) extracted by Goldhammer and Harris [38] from the Latemar stratigraphy is a consequence of variation in (non-linear) tectonic subsidence rather than being a eustatic signal.

(2) Another possible source of non-periodic modulation of potentially periodic base signals in the South Alpine realm are the multiple fallout events of volcaniclastics related to the Pietra Verde eruptions. Around 40 distinct volcaniclastic layers have been detected to date throughout the entire pelagic succession of the Buchenstein Beds in the northwestern Dolomites (see Seceda column in Fig. 2), but the real number of volcanic events might have been considerably higher. Recent discovery of tuff layers up to several centimetres thick and at different levels of platform-interior beds at Latemar indicate that such events did result in distinct bedding planes. Their recognition and identification within the several hundred meter thick platform succession is, however, difficult.

Based on our age constraints and in view of the various possible mechanisms resulting in or modifying carbonate stacking patterns, we doubt that evidence provided from spectral analysis alone can furnish adequate proof of orbital tuning control for the sedimentation patterns recognized in the Latemar carbonate platform. Only a combined effort by robust spectral analysis, high-resolution age calibration and detailed study of equivalent sections in other platforms of this area might finally result in a more comprehensive model.

Acknowledgements

This work was founded by Swiss National Science Foundation grant 20-35914.92. We are indebted to R.H. Steiger for his generous support throughout this study. The assistance of H. Derksen and R. Bickel with mineral separation and preparation is gratefully acknowledged. We also benefited from the help of S. Bernasconi in sample collection and advice in the field. For thorough reviews and helpful

suggestions we wish to thank M.A. Arthur, J.N. Connelly and W. Schlager. *[MK]*

Appendix A. Analytical procedures

All U–Pb age determinations were performed at the isotope laboratory of the Institute of Isotope Geology and Mineral Resources (IGMR) at ETH Zürich. Rock samples weighing 5–25 kg were collected with great care in order to avoid contamination from adjoining layers. For massive, unweathered Pietra Verde samples, crushers, mills and Wilfley table were used to obtain a heavy mineral enriched fraction. Bentonites and strongly weathered samples were disintegrated in dilute acetic acid using an ultrasonic disintegrator. Mineral concentrates were then purified by standard heavy-liquid and magnetic separation techniques. Individual zircon grains were pre-selected using a binocular microscope. These grains were then examined by transmitted light microscopy. Only euhedral, clear grains devoid of optically recognizable cores were chosen for analysis to avoid components predating the deposition age. Furthermore, grains with cracks were also excluded from analysis as they may preferentially be affected by secondary Pb loss. To minimize surface-correlated secondary lead loss further, the majority of the crystals were subjected to step-wise air abrasion [11]. The reduction in volume was checked by measuring the smallest diameter (listed in Table 1). Fig. 6 clearly shows a correlation between the reduction in volume and the degree of discordance for the 60 zircons measured in this study. Typically, a reduction of 20% with respect to the smallest diameter was sufficient to remove most crystal portions affected by Pb loss. However, even in the case of strongly abraded grains, the problem of Pb loss cannot entirely be avoided. Selected grains showed approximately equal proportions of the {101} and {211} pyramids, and, with the exception of sample BAG.07, a dominance of the {100} prism. The morphological characteristics of the zircon populations from all samples are compiled in Fig. 7, using the classification of Pupin [39].

Sample preparation, chemical processing and mass spectrometric measurements were performed following the methods described in detail by Meier and Oberli in [29]. The small sample size resulting from abrasion, in combination with moderate U concentrations, required the analysis of radiogenic Pb amounts as low as 3.2 pg. Consequently, analytical blanks had to be controlled at low level. In the course of the study, the amount of laboratory common Pb contamination decreased from 4.9 ± 2.2 to 2.4 ± 0.6 pg per analysis due to improved reagents. Corrections for laboratory blank are based on the following mea-

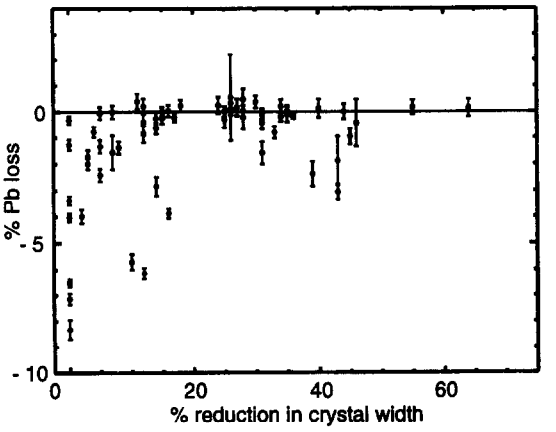

Fig. 6. Correlation between reduction in width by air abrasion and degree of discordance for 60 zircons analyzed in this study.

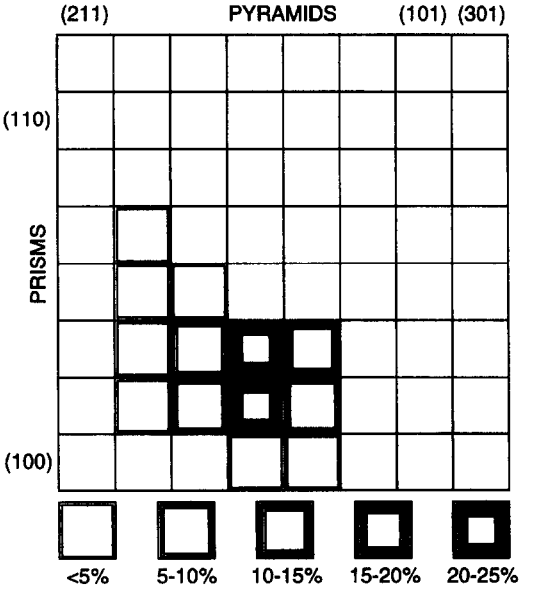

Fig. 7. Morphological characterization of all zircons examined in this study using the classification diagram of [39].

sured isotopic ratios and reproducibilities: $^{208}Pb/^{206}Pb = 2.067 \pm 0.023$, $^{207}Pb/^{206}Pb = 0.852 \pm 0.015$, $^{204}Pb/^{206}Pb = 0.0551 \pm 0.0013$ (reproducibilities given at the 2σ level). Corrections for sample common Pb are based on the following Pb isotopic compositions: $^{208}Pb/^{204}Pb = 38.191$, $^{207}Pb/^{204}Pb = 15.69$, $^{206}Pb/^{204}Pb = 18.333$ (240 Ma; [26] model III). No errors were assigned to these model values, as even large variations in common Pb composition would cause only negligible shifts in the final age result. In all samples $^{206}Pb_{rad}/^{206}Pb_{tot}$ is sufficiently high for precise $^{206}Pb/^{238}U$ age results to be obtained.

Appendix B. Processing of data obtained on non-ideal isotopic systems

Secondary (post-depositional) loss of radiogenic Pb of zircons from sedimentary environments causes a dispersion of the $^{206}Pb/^{238}U$ and $^{207}Pb/^{235}U$ ages. If the shift to lower Pb/U ratios is relatively large and the data are precise enough, the data points represented by their error ellipses become resolved from the Concordia curve (e.g., Z105 in Fig. 3). As radiogenic ^{207}Pb in early Mesozoic zircons is about 20 times less abundant than ^{206}Pb, small samples will show considerable uncertainties in $^{207}Pb/^{235}U$ (e.g., ~ 10% for Z107, Table 1 and Fig. 3). For these samples, concordancy (Pb/U ratios equal within error limits) no longer serves as a useful criterion for the distinction of undisturbed from disturbed isotopic systems. For these cases, dispersion of the ages can more readily be recognized from the scatter of the much more precise $^{206}Pb/^{238}U$ ratios alone, which usually have precisions $< 0.5\%$.

The dispersion of the data is reduced or eliminated by careful selection of higher quality crystals combined with controlled abrasion. In favourable cases tight data clusters are obtained (Fig. 3). For the calculation of mean values, data points which are clearly resolved from the concordia curve or from the clusters defined by the $^{206}Pb/^{238}U$ ages were excluded. Similarly, insufficiently abraded samples were omitted in order to avoid bias of the results to lower age values (see text).

Mean ages and their uncertainties calculated by three different methods from the $^{206}Pb/^{238}U$ data are compared in Table 2. All errors are given at the 95% confidence level. Standard least-squares techniques were used to obtain the mean values given in column 1 and associated statistical parameters (columns 2–4), weighing the individual values by $1/s^2$. Column 2 shows 'internal' uncertainties derived by error propagation, whereas 'external' uncertainties (column 3) were calculated from the scatter of the data. At the 95% confidence level the MSWD values listed in column 4 cannot be distinguished from the expected value of 1; that is, no scatter in excess of analytical uncertainties is resolved in the data sets selected for calculation of the means. It must, however, be emphasized that the data sets used are very small. Particular attention must be paid to the fact that data affected by secondary Pb loss are not normally distributed. This calls for application of distribution-free statistical methods which are less sensitive to deviations from normal distribution, such as a symmetry of the data sets. Columns 5 and 6 contain median values and confidence intervals based on the Wilcoxon sign test (see [40]), respectively. Inspection of all data listed in Table 2 clearly shows that the means and associated uncertainties calculated by different methods do not significantly differ. The interpretation of the age results is, therefore, rather independent from the particular method used. Preference is given to the distribution-independent method. The results are therefore given as the median and associated uncertainties calculated from the Wilcoxon sign test.The alternative method of determining the primary crystallization age of discordant zircon data from the intercept of best-fit lines with the concordia curve results in uncertainties which are an order of magnitude higher than the errors obtained by the clustering procedure, due to large errors in $^{207}Pb/^{235}Pb$ and low-angle intercept relationships. Calculations carried out for all five samples showed that the lower intercepts are indistinguishable from zero age within their (large) error brackets.

References

[1] A.R. Palmer (Compiler), Decade of North American Geology (DNAG), Geologic time scale, Geology 11, 503–504, 1983.
[2] S.C. Forster and G. Warrington, Geochronology of the Carboniferous, Permian and Triassic, in: The Chronology of the

Geological Record, N.J. Snelling, ed., Geol. Soc. London Mem. 10, 99–113, 1985.
[3] G.S. Odin, Geological time scale, C. R. Acad. Sci. Paris, 318/II, 59–71, 1994.
[4] F.M. Gradstein, F.P. Agterberg, J.G. Ogg, J. Hardenbol, P. van Veen, J. Thierry and Zehui Huang, A Mesozoic time scale, J. Geophys. Res. 99/12, 24051–24074, 1994.
[5] R.K. Goldhammer, P.A. Dunn and L.A. Hardie, High frequency glacio-eustatic sea level oscillations with Milankovitch characteristics recorded in Middle Triassic platform carbonates in northern Italy, Am. J. Sci. 287, 853–892, 1987.
[6] L.A. Hinnov and R.K. Goldhammer, Spectral analysis of the Middle Triassic Latemar Limestone, J. Sed. Petrol. 61/7, 1173–1193, 1991.
[7] W.B. Harland, R.L. Armstrong, A.V. Cox, L.E. Craig, A.G. Smith and D.G. Smith, A Geologic Time Scale 1989, 265 pp., Cambridge University Press, New York, 1990.
[8] K.N. Hellmann and H.J. Lippolt, Calibration of the Middle Triassic time scale by conventional K–Ar and $^{40}Ar/^{39}Ar$ dating of alkali feldspars, J. Geophys. 50, 73–86, 1981.
[9] S. Borsi and G. Ferrara, Determinazione dell'età delle rocce intrusive di Predazzo con i metodi del Rb/Sr e del K/Ar, Miner. Petrogr. Acta 13, 45–65, 1967.
[10] S. Borsi, G. Ferrara, L. Paganelli and G. Simboli, Isotopic age measurement of the M. Monzoni intrusive complex, Miner. Petrogr. Acta 14, 171–183, 1968.
[11] T.E. Krogh, Improved accuracy of U–Pb zircon ages by the creation of more concordant systems using an air abrasion technique, Geochim. Cosmochim. Acta 46, 637–649, 1982.
[12] P. Brack and H. Rieber, Towards a better definition of the Anisian/Ladinian boundary: New biostratigraphic data and correlations of boundary sections from the Southern Alps, Eclog. Geol. Helv. 86, 415–527, 1993.
[13] E. Callegari and A. Monese, Il chimismo della "pietra verde" degli Strati di Livinallongo (Dolomiti). Contributo allo studio petrogenetico della "pietra verde" ladinica, Stud. Trent. Sci. Nat. 41/1, 45–71, 1964.
[14] P. Gianolla, Eruzione freatomagmatica di grande magnitudo nel Ladinico delle Dolomiti (Nota preliminare), Rend. Soc. Geol. Ital. 14, 65–70, 1991.
[15] A. Bosellini, Progradation geometries of carbonate platforms: Examples from the Triassic of the Dolomites, northern Italy, Sedimentology 31, 1–24, 1984.
[16] A.G. Fischer, The Lofer cyclothems of the Alpine Triassic, Kansas Geol. Surv. Bull. 169, 107–149, 1994.
[17] J.D. Hays, J. Imbrie and N.J. Shackleton, Variations in the earth's orbit: Pacemaker of the ice ages, Science 194/4270, 1121–1132, 1976.
[18] M. Milankovitch, Kanon der Erdbestrahlung und seine Anwendung auf das Eiszeitenproblem. R. Serb. Acad. Sci. Spec. Publ. 132, Section of Mathematical and Natural Sciences 33, 1941.
[19] P. Brack and H. Rieber, The Anisian/Ladinian boundary: retrospective and new constraints, Albertiana 13, 25–36, 1994.
[20] P. Brack, H. Rieber and R. Mundil, The Anisian/Ladinian boundary interval at Bagolino (Southern Alps, Italy): I. Summary and new results on ammonoid horizons and radiometric age dating, Albertiana 15, 45–56, 1995.
[21] A. Nicora and P. Brack, The Anisian/Ladinian boundary interval at Bagolino (Southern Alps, Italy): II. The distribution of conodonts, Albertiana 15, 57–65, 1995.
[22] H. Bucher and M.J. Orchard, Intercalibrated ammonoid and conodont succession, Upper Anisian–Lower Ladinian of Nevada, Albertiana 15, 66–70, 1995.
[23] S.M. Bernasconi, Geochemical and microbial controls on dolomite formation in anoxic environments: A case study from the Middle Triassic (Ticino, Switzerland), Contrib. Sedimentol. 19, 109 pp., 1994.
[24] W. Müller, R. Schmid and P. Vogt, Vulkanogene Lagen aus der Grenzbitumenzone (Mittlere Trias) des Monte San Giorgio in den Tessiner Kalkalpen, Eclog. Geol. Helv. 57, 431–450, 1964.
[25] H. Rieber, Cephalopoden aus der Grenzbitumenzone (Mittlere Trias) des Monte San Giorgio (Kanton Tessin, Schweiz), Schweiz. Paläont. Abh. 93, 1–96, 1973.
[26] G.L. Cumming and J.R. Richards, Ore lead isotope ratios in a continuously changing earth, Earth Planet. Sci. Lett. 28, 155–171, 1975.
[27] R.H. Steiger, R.A. Bickel and M. Meier, Conventional U–Pb dating of single fragments of zircon for petrogenetic studies of Phanerozoic granitoids, Earth Planet. Sci. Lett. 115, 197–209, 1993.
[28] P.A. Scholle, M.A. Arthur and A.A. Ekdale, Pelagic environment, in: Carbonate Depositional Environments, P.A. Scholle, D.G. Bebout and C.H. Moore, eds., AAPG Mem. 33, 619–691, 1983.
[29] M. Wiedenbeck, P. Allé, F. Corfu, W.L. Griffin, M. Meier, F. Oberli, A. von Quadt, J.C. Roddick and W. Spiegel, Three natural zircon standards for U–Th–Pb, Lu–Hf, trace element and REE analyses, Geostand. Newsl. 19, 1–23, 1995.
[30] C.M. Crisci, G. Ferrara, R. Mazzuoli and P.M. Rossi, Geochemical and geochronological data on Triassic volcanism of the Southern Alps of Lombardy (Italy): genetic implications, Geol. Rundsch. 73, 279–292, 1984.
[31] M. Gaetani, Working Group on Anisian, Ladinian and Carnian Stage Boundaries, Albertiana 14, 51–53, 1994.
[32] A. Dagis and W. Weitschat, Correlation of the Boreal Triassic, Mitt. Geol.-Paläont. Inst. Univ. Hamburg 75, 249–256, 1993.
[33] P.M. van Veen, L.J. Skjold, S.E. Kristensen, A. Rasmussen, J. Gjelberg and T. Stølan, Triassic sequence stratigraphy in the Barents Sea, in: Arctic Geology and Petroleum Potential, T.O. Vorren, E. Bergsager, Ø.A. Dahl-Stamnes, E. Holter, B. Johansen, E. Lie and T.B. Lund, eds., NPF Spec. Publ. 2, 515–538, 1992.
[34] J.C. Claoué-Long, Zhang Zichao, Ma Guogan and Du Shaohua, The age of the Permian–Triassic boundary, Earth Planet. Sci. Lett. 105, 182–190, 1991.
[35] P. Brack, R. Mundil, M. Meier, F. Oberli and H. Rieber, Biostratigraphic and radiometric age data question the Milankovitch characteristics of the Latemar cycles (Southern Alps, Italy), Geology, 1996 (in press).

[36] A. Berger, M.F. Loutre and J. Laskar, Stability of the astronomical frequencies over the earth's history for paleoclimate studies, Science 255, 560–566, 1992.

[37] C.N. Drummond and B.H. Wilkinson, Carbonate cycle stacking patterns and hierarchies of orbitally forced eustatic sealevel change, J. Sediment. Petrol. 63, 369–377, 1993.

[38] R.K. Goldhammer and M.T. Harris, Eustatic controls on the stratigraphy and geometry of the Latemar buildup (Middle Triassic), the Dolomites of Northern Italy, in: Controls on Carbonate Platform and Basin Development, P.D. Crevello, J.F. Sarg, J.F. Read and J.L. Wilson, eds., SEPM Spec. Publ. 44, 323–338, 1989.

[39] J.P. Pupin, Zircon and granite petrology, Contrib. Mineral. Petrol. 73, 207–220, 1980.

[40] N.M.S. Rock, J.A. Webb, N.J. McNaughton and G.D. Bell, Nonparametric estimation of averages and errors for small data-sets in isotope geoscience: A proposal, Chem. Geol. 66, 163–177, 1982.

ELSEVIER

Earth and Planetary Science Letters 143 (1996) 275

EPSL

Erratum

Erratum to "High resolution U–Pb dating of Middle Triassic volcaniclastics: Time-scale calibration and verification for tuning parameters for carbonate sedimentation" [Earth Planet. Sci. Lett. 141 (1996) 137–151] [1]

Roland Mundil, Peter Brack, Martin Meier, Hans Rieber, Felix Oberli

Due to technical faults in our Production Department an error has occurred in the presentation of Fig. 4 (p. 145) of the above paper. On the position of Fig. 4, Fig. 6 was duplicated from p. 148. The correct and original Fig. 4 follows below. We apologize for any inconvenience caused.

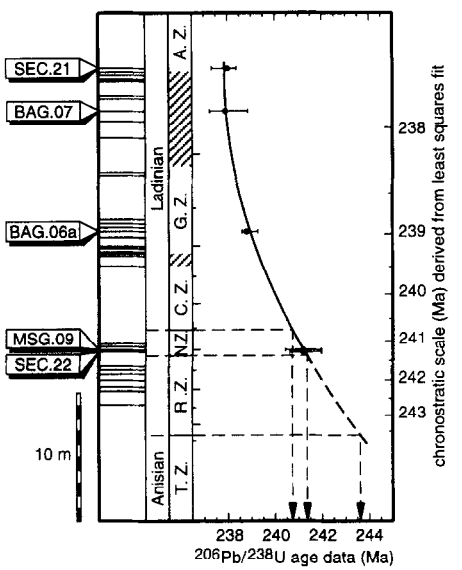

Fig. 4. Second-order least-squares fit of age data. The Bagolino section was taken as reference. The thickness of all volcaniclastic layers is reduced to zero. Arrows mark potential biostratigraphic collocations of the Anisian/Ladinian boundary and corresponding numeric ages.

[1] PII of original article: S0012-821X(96)00057-X.

PII S0012-821X(96)00147-1